

peak responding to the two frequency components that contribute to it. The sideband peak profile will thus show modulation with τ if phase differences vary over the bandwidth. Such profile changes are not apparent in our data, hence the harmonics must be frequency-modulated ("chirped") in a similar way. An identical chirp in all harmonics does not affect the intensity envelope of the attosecond pulses, only the phase of their carrier wave (which we cannot measure).

The experimental evidence presented here for the existence of attosecond pulses in the process of HHG confirms theoretical predictions that the natural phase with which groups of neighboring harmonics are generated is sufficient to cause such pulse trains. In addition, our technique of phase measurement is a general one, applicable to deep in the extreme ultraviolet, and scales without difficulty to larger groups of harmonics. A measurement scheme for the phases may enable their purposeful manipulation (e.g., through dispersion when propagating through a gas cell), even if the harmonics were initially generated with undesirable phases. With such techniques, it should ultimately become possible to properly phase all harmonics emerging from the generation jet, leading to pulses perhaps as short as 10 as. The generation of these pulses still must be investigated in more detail, and ways of control and selection must be developed, before attosecond pulses can be routinely used as light sources in experiments.

References and Notes

1. P. Salières, A. L'Huillier, P. Antoine, M. Lewenstein, in *Advances in Atomic, Molecular, and Optical Physics*, B. Bederson, H. Walther, Eds. (Academic Press, New York, 1999), vol. 41, p. 83.
2. A. E. Kaplan, *Phys. Rev. Lett.* **73**, 1243 (1994).
3. A. V. Sokolov, D. R. Walker, D. D. Yavuz, G. Y. Yin, S. E. Harris, *Phys. Rev. Lett.* **85**, 562 (2000).
4. M. Ivanov, P. B. Corkum, T. Zuo, A. Bandrauk, *Phys. Rev. Lett.* **74**, 2933 (1995).
5. P. B. Corkum, *Phys. Rev. Lett.* **71**, 1994 (1993).
6. M. Lewenstein, P. Balcou, M. Ivanov, A. L'Huillier, P. B. Corkum, *Phys. Rev. A* **49**, 2117 (1994).
7. W. Becker, A. Lohr, M. Kleber, M. Lewenstein, *Phys. Rev. A* **56**, 645 (1997).
8. T. Sekikawa, T. Ohno, T. Yamazaki, Y. Nabekawa, S. Watanabe, *Phys. Rev. Lett.* **83**, 2564 (1999).
9. E. S. Toma *et al.*, *Phys. Rev. A* **62**, 061801(R) (2000).
10. M. Drescher *et al.*, *Science* **291**, 1923 (2001).
11. G. Farkas, C. Toth, *Phys. Lett. A* **168**, 447 (1992).
12. S. E. Harris *et al.*, *Opt. Commun.* **100**, 487 (1993).
13. P. Antoine, A. L'Huillier, M. Lewenstein, *Phys. Rev. Lett.* **77**, 1234 (1996).
14. P. Antoine *et al.*, *Phys. Rev. A* **56**, 4960 (1997).
15. I. P. Christov, M. M. Murnane, H. C. Kapteyn, *Phys. Rev. A* **57**, 2285 (1998).
16. N. A. Papadogiannis, B. Witzel, C. Kalpouzos, D. Charalambidis, *Phys. Rev. Lett.* **83**, 4289 (1999).
17. V. Veniard, R. Taieb, A. Maquet, *Phys. Rev. A* **54**, 721 (1996).
18. J. M. Schins *et al.*, *J. Opt. Soc. Am. B* **13**, 197 (1996).
19. The rotating-wave approximation is used.
20. S. Klarsfeld, A. Maquet, *J. Phys. B* **12**, L553 (1979).
21. M. Aymar, M. Crance, *J. Phys. B* **13**, L287 (1980).
22. The turn-on boundary condition prescribes in ω_2 an infinitesimal positive imaginary part $i\eta$, which defines the integral in the spectral representation of $(E - H)^{-1}$ as a (real) principal-value integral minus an imaginary delta function $i\pi\delta(E - H)$.

23. The plates could be aligned parallel with each other within a precision of 0.01°. The path of any of the beams through its plate depends on the incidence angle, which can be changed by rotating the plate. The plate responsible for the delay of the central part of the beam is mounted on a computer-controlled rotation stage, which can make steps of 0.005°. Very small delays can be achieved with it, because close to the normal incidence, the time delay has second-order dependence on the incidence angle. Given the dimensions of our plates, a tilt of 1° produces a delay of 1 fs of the pulse.
24. The standard deviation in these phases is about 0.3 radian.
25. The amplitude of the 11th harmonic was not directly measured. Because the modulation depths of all side-

bands are similar, we can conclude that harmonic 11 is not much different from harmonic 13 in intensity. In the calculations we used a value 1.5 times that of the 13th-harmonic magnitude. Had this ratio been 0.5, the peak FWHM in Fig. 4 would have been only slightly longer.

26. This work is part of the research program of FOM (Fundamental Research on Matter), which is subsidized by NWO (Netherlands Organization for the Advancement of Research). It was also supported by the European Commission (Access Contract HPRI-CT-1999-00086) and by the EC's Training and Mobility of Researchers program (contract HPRN-CT-2000-00133). We thank V. Veniard, R. Taieb, A. Maquet, and E. Constant for useful discussions.

30 January 2001; accepted 20 April 2001

Anomalous Weak Magnetism in Superconducting $\text{YBa}_2\text{Cu}_3\text{O}_{6+x}$

J. E. Sonier,^{1,3*} J. H. Brewer,^{2,3} R. F. Kiefl,^{2,3} R. I. Miller,² G. D. Morris,³ C. E. Stronach,⁴ J. S. Gardner,⁵ S. R. Dunsiger,^{2†} D. A. Bonn,² W. N. Hardy,² R. Liang,² R. H. Heffner⁶

For some time now, there has been considerable experimental and theoretical effort to understand the role of the normal-state "pseudogap" phase in underdoped high-temperature cuprate superconductors. Recent debate has centered on the question of whether the pseudogap is independent of superconductivity. We provide evidence from zero-field muon spin relaxation measurements in $\text{YBa}_2\text{Cu}_3\text{O}_{6+x}$ for the presence of small spontaneous static magnetic fields of electronic origin intimately related to the pseudogap transition. Our most significant finding is that, for optimal doping, these weak static magnetic fields appear well below the superconducting transition temperature. The two compositions measured suggest the existence of a quantum critical point somewhat above optimal doping.

Of the high-temperature cuprate superconductors, $\text{YBa}_2\text{Cu}_3\text{O}_{6+x}$ has been the most widely studied. The parent compound, $\text{YBa}_2\text{Cu}_3\text{O}_6$, is an antiferromagnetic (AF) insulator that becomes a superconductor with hole (oxygen) doping. Nuclear magnetic resonance (NMR) (I), inelastic neutron scattering (2), and muon spin relaxation (μSR) (3–6) studies clearly show that short-range AF correlations of the Cu spins in the CuO_2 planes persist for hole concentrations well beyond the three-dimensional AF phase, leading some to suspect a spin-fluctuation pairing mechanism for superconductivity. Recently, the onset of spin fluctuations above the superconducting transition tem-

perature T_c has been linked to the formation of the pseudogap (7), first observed (8) as a gap in the spin-excitation spectrum of $\text{YBa}_2\text{Cu}_3\text{O}_{6.7}$ and later identified as a coinciding gap in the quasiparticle-excitation spectrum (9). Early interpretations of the pseudogap favored a scenario in which phase-incoherent pairing correlations (10), established in the normal state at a crossover temperature T^* , condense into the coherent superconducting state below the transition temperature T_c . Experiments showing that the pseudogap above T_c evolves continuously into the superconducting gap below T_c lent strong support to this idea. However, a careful examination by Tallon and Loram (11) of several key experiments supports an alternative view, whereby the pseudogap is in fact distinct from the superconducting gap, and the temperature T^* defines an energy scale that vanishes ($T^* \rightarrow 0$) in the slightly overdoped region at a critical point $p_{cr} \approx 0.19$ (where p is the fraction of holes per Cu atom in the CuO_2 plane). A crucial observation is that short-range AF correlations persist at temperatures above 0 K at the critical hole concentration $p_{cr} = 0.19$.

Consistent with the latter view, several groups have proposed that there is another source of magnetism, which is distinct from the Cu-spin magnetism and more intimately asso-

¹Department of Physics, Simon Fraser University, Burnaby, British Columbia V5A 1S6, Canada. ²Department of Physics and Astronomy, University of British Columbia, Vancouver, British Columbia V6T 1Z1, Canada. ³TRIUMF, Vancouver, British Columbia V6T 2A3, Canada. ⁴Department of Physics, Virginia State University, Petersburg, VA 23806, USA. ⁵National Research Council, Chalk River, Ontario K0J 1P0, Canada. ⁶Los Alamos National Laboratory, Los Alamos, NM 87545, USA.

*To whom correspondence should be addressed. E-mail: jeff_sonier@sfu.ca
 †Present address: Department of Physics and Astronomy, University of California Los Angeles, Los Angeles, CA 90095, USA.

ciated with the pseudogap phase. Early on, Varma (12, 13) developed a model that describes T^* as a crossover to a phase with broken time and rotational symmetry, in which a fourfold pattern of circulating current (CC) flows in the basal (a, b) plane. The CC phase terminates ($T^* \rightarrow 0$) at a critical point p_{cr} within the superconducting region of the $T-p$ phase diagram. More recently, Chakravarty *et al.* (14) have proposed a similar picture whereby the pseudogap phase is characterized by the development of a new order parameter, a so-called $d_{x^2-y^2}$ density wave (DDW) state. At temperatures below T^* , circulating currents associated with the time-reversal breaking DDW phase produce local magnetic fields that point along the \hat{c} -direction at the apical oxygen sites. Like the CC phase, the DDW phase vanishes at a critical doped-hole concentration p_{cr} under the superconducting “dome.” A key property of the DDW transition is that it is strongly suppressed by disorder. Thus, only clean samples are expected to show a true phase transition at T^* corresponding to the onset of DDW order.

We note that physical magnetic fields arising from circulating electronic currents were first introduced as a property of the so-called staggered flux phase of the $t-J$ model (15), which competes with $d_{x^2-y^2}$ -wave superconductivity. According to Wen and Lee, the fluctuating staggered current loops are stabilized only in a magnetic field that is large enough to suppress the superconducting order (16). However, it has been shown that the addition of off-site Coulomb repulsion to the pure $t-J$ model leads to ordering of the staggered flux phase in zero external field (17). Of the various models that predict spontaneous magnetic fields associated with a time-reversal breaking phase, only the proposed CC phase preserves the translational symmetry of the underlying lattice.

The zero-field muon spin relaxation (ZF- μ SR) technique offers the opportunity to observe the onset of weak spontaneous magnetic fields at the pseudogap crossover in the $\text{YBa}_2\text{Cu}_3\text{O}_{6+x}$ system. The spin of the positive muon can detect static internal magnetic fields on the order of 0.1 G (18). Moreover, the technique can easily distinguish such static fields from relaxation due to the rapid Cu spin fluctuations observed with neutron scattering in the vicinity of T^* . Earlier ZF- μ SR studies of the $\text{YBa}_2\text{Cu}_3\text{O}_{6+x}$ system (6) show that static magnetic order persisting from the AF phase is absent beyond $x \approx 0.5$. Measurements on an $x = 1$ polycrystalline sample found no clear evidence for the onset of spontaneous internal magnetic fields at or below T_c (19). However, recent neutron scattering experiments on underdoped $x = 0.5$ (20) and $x = 0.6$ (21) samples of $\text{YBa}_2\text{Cu}_3\text{O}_{6+x}$ have identified the onset of previously undetected magnetism at temperatures well above T_c . The observed weak magnetic moments, argued to be distinct from the well-known Cu spin magnetism, are consistent with

an orbital current phase that breaks translational symmetry of the lattice. Although this finding appears to be compatible with the DDW and staggered flux phase pictures, angle-resolved photoemission spectroscopy (ARPES) studies have yet to show clear evidence for the existence of Fermi surface hole pockets, which are a feature characteristic of these same theoretical models. Consequently, the origin of the weak moments observed with neutron scattering is currently unknown.

Here, we report on ZF- μ SR measurements of $\text{YBa}_2\text{Cu}_3\text{O}_{6+x}$ single crystals, using the HELIOS and LAMPF spectrometers on the M20 surface muon beam line at the TRI-University Meson Facility (TRIUMF) (22). Optimally doped $x = 0.95$ crystals with $T_c = 93.2 \pm 0.3$ K were prepared by a flux method in yttria-stabilized zirconia crucibles (23). Detwinned ortho-III phase $x = 0.67$ crystals with $T_c = 67.9 \pm 1.2$ K were grown by a flux method using BaZrO_3 crucibles, following the same procedure used to grow ortho-II phase crystals (24). The ortho-III phase is characterized by a unit cell consisting of one completely deoxygenated and two consecutive fully oxygenated CuO chains in the basal plane. Underdoped crystals containing CuO chains that are completely full or empty have optimum oxygen homogeneity and minimal opportunity for phase separation in the oxygen annealing process.

The muons were implanted into the bulk of the sample with their initial spin polarization $\hat{P}_\mu(0)$ parallel (\parallel) or perpendicular (\perp) to the \hat{c} -axis of the crystals. Figure 1 shows the measured time evolution of the muon spin polarization in the $x = 0.95$ crystals in zero applied magnetic field for the case $\hat{P}_\mu(0) \perp \hat{c}$. The parameter a is the initial muon-decay asymmetry at time $t = 0$, which depends mainly on the energies of the detected positrons and the solid angles subtended by the detectors. At 115 K and below T_c at 55 K, the ZF time spectra are identical, confirming the earlier work (19) in which no evidence was found for the appearance of spontaneous internal magnetic fields upon cooling through T_c . The solid curve (Fig. 1A) is a fit to the well-known Kubo-Toyabe function (25) that describes the depolarization (or relaxation) of the muon spin by the randomly orientated static magnetic fields of the nuclear dipoles

$$G_z^{\text{KT}}(t) = \frac{1}{3} + \frac{2}{3} (1 - \Delta^2 t^2) \exp\left(-\frac{1}{2} \Delta^2 t^2\right) \quad (1)$$

where Δ/γ_μ is the width of the Gaussian field distribution at the muon site and $\gamma_\mu = 0.0852 \mu\text{s}^{-1} \text{G}^{-1}$ is the muon gyromagnetic ratio. The first term, which does not evolve in time, corresponds to the 1/3 component of the initial muon-spin polarization (defined to be along the z -direction) that is parallel to the local field.

This is not evident in the time spectra, because for $\Delta t \ll 1$ (early time and/or small Δ) the Kubo-Toyabe function reduces to a simple Gaussian form $G_z^{\text{KT}}(t) \approx \exp(-\Delta^2 t^2)$. The fit to Eq. 1 yields $\Delta_\perp = 0.1144 \pm 0.0006 \mu\text{s}^{-1}$. The line width parameter Δ is expected to be independent of temperature below 200 K where the muon is immobile (19).

On cooling below 45 ± 10 K (Fig. 1B), there is a marked increase in the ZF relaxation rate, signifying the occurrence of a small additional magnetic field at the muon site(s). The time evolution of the muon spin polarization below 45 K was better described by the product of Eq. 1 and an exponential function, $G_z(t) = G_z^{\text{KT}}(t) \cdot \exp(-\lambda t)$, which arises if there is an additional source of magnetic field that convolutes with the field distribution of the nuclear dipoles. The temperature dependence of the exponential relaxation rate λ was determined on separate occasions with the HELIOS and LAMPF spectrometers (Fig. 2A). The error bars represent the statistical uncertainty in the fits, whereas the random scatter of the data is due to small instrumental effects related to variations in the incoming muon rate. No observable change is seen at T_c , indicating that any stray field present in the normal state is well below the limit of detection. The sudden increase in the relaxation rate below about 45 K is also observed for the case $\hat{P}_\mu(0) \parallel \hat{c}$ (Fig. 2B), although with this orientation of the muon spin, λ has a smaller maximum value at the lowest tempera-

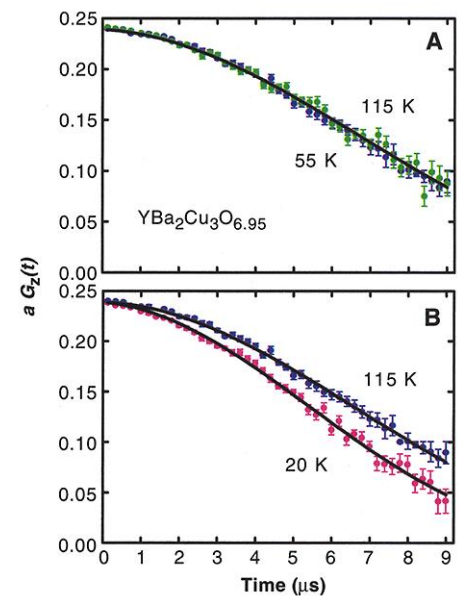


Fig. 1. The time evolution of the muon spin polarization in zero external field for $\text{YBa}_2\text{Cu}_3\text{O}_{6.95}$ crystals, measured with the initial muon spin polarization $\hat{P}_\mu(0)$ perpendicular to the \hat{c} -axis. (A) Measurements taken above T_c at 115 K (blue circles) and below T_c at 55 K (green circles). The solid curve is a fit to Eq. 1. (B) Measurements taken above and below T_c at 115 K (blue circles) and 20 K (magenta circles), respectively. The solid curve through the 20 K data is a fit to Eq. 2.

ture considered. Fits of the ZF time spectra at higher temperatures for this latter orientation yield $\Delta_{\parallel} = 0.1065 \pm 0.0008 \mu\text{s}^{-1}$. We note that the anisotropy ratio $\Delta_{\perp}/\Delta_{\parallel} \approx 1.07$ is significantly smaller than the ratio $\lambda_{\perp}/\lambda_{\parallel} \approx 1.70$ at the lowest temperature.

In order to confirm that the increase in the

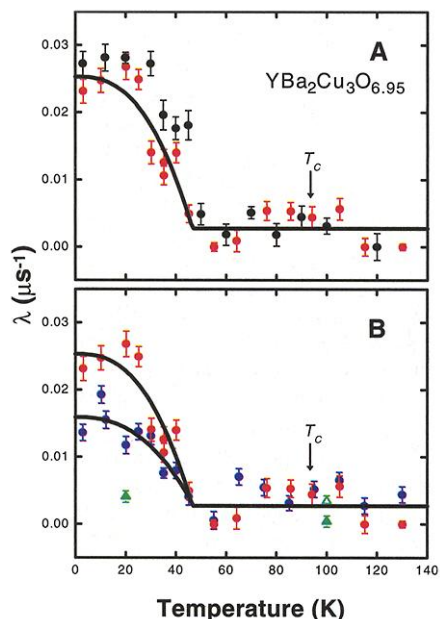
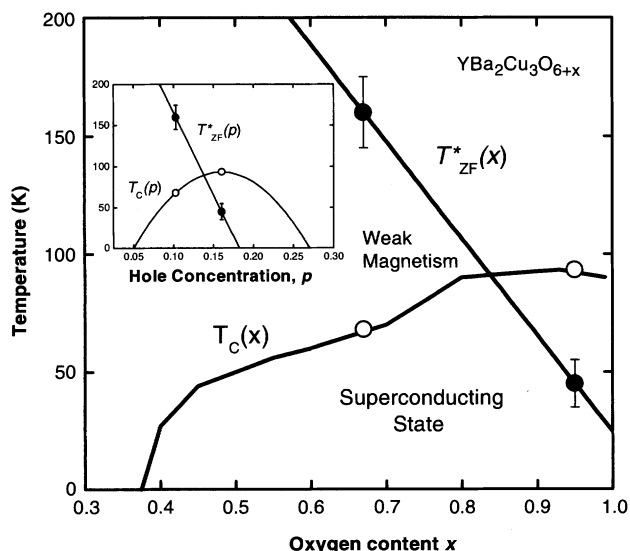


Fig. 2. The temperature dependence of the ZF exponential relaxation rate λ (see Eq. 2) in $\text{YBa}_2\text{Cu}_3\text{O}_{6.95}$. (A) Measurements taken with the HELIOS (black circles) and LAMPF (red circles) spectrometers with the initial muon spin polarization $\hat{P}_{\mu}(0)$ perpendicular to the \hat{c} -axis. (B) Measurements taken with the LAMPF spectrometer with $\hat{P}_{\mu}(0)$ perpendicular (red circles) and parallel (blue circles) to the \hat{c} -axis. The solid curves are guides to the eye. Also shown are LF measurements in an applied magnetic field of 0.5 kOe (solid green triangles) and 1.0 kOe (open green triangle) taken with $\hat{P}_{\mu}(0)$ parallel to the \hat{c} -axis.

Fig. 4. The temperature versus oxygen content x phase diagram for $\text{YBa}_2\text{Cu}_3\text{O}_{6+x}$. The open circles are the superconducting transition temperature (T_c) of the $x = 0.67$ and $x = 0.95$ crystals. The solid curve through these data points is from (34). The solid circles indicate the temperature $T_{\text{ZF}}^*(x)$ at which the onset of a spontaneous magnetic field is observed in the ZF- μSR time spectra. The solid line is a linear fit to these points. (Inset) The corresponding phase diagram of temperature versus hole concentration p . The solid curve through the data points for $T_c(p)$ is Eq. 3. The solid line through the data points for $T_{\text{ZF}}^*(p)$ is a linear fit extrapolated to $T = 0$, yielding $p_{\text{cr}} = 0.182 \pm 0.009$.



exponential relaxation rate below about 45 K is due to small static internal local fields, rather than to slowing down of the fast Cu spin fluctuations, we carried out measurements above and below 45 K with a longitudinal field (LF) of 0.5 kOe applied along the initial direction of the muon spin (for the case $\hat{P}_{\mu}(0) \parallel \hat{c}$). A field was chosen that was large enough so that magnetic flux could penetrate the interior of the sample in the form of a vortex lattice. The LF completely decouples the effect of the static nuclear dipoles [$G_z^{\text{KT}}(t) \rightarrow 1$] and strongly reduces λ_{\parallel} below 45 K (Fig. 2B), indicating that the muon spin is fully decoupled from the local fields. The observed increase of λ_{\parallel} in ZF is therefore attributed to a static or quasi-static (i.e., field fluctuation frequency < 1 MHz) local field distribution at the muon site. Although the data have been fit to an exponential relaxation function, the increased relaxation is too small to clearly distinguish between an exponential function characteristic of a dilute con-

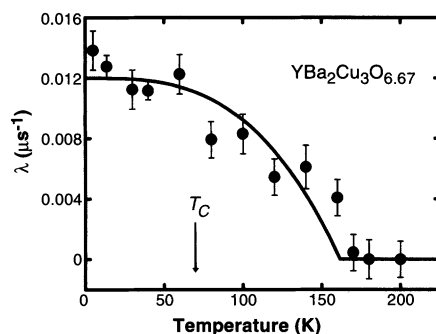


Fig. 3. The temperature dependence of the ZF exponential relaxation rate λ in $\text{YBa}_2\text{Cu}_3\text{O}_{6.67}$ measured with the LAMPF spectrometer and the initial muon spin polarization $\hat{P}_{\mu}(0)$ perpendicular to the \hat{c} -axis. The solid curve is a guide to the eye.

centration of magnetic moments and forms of the relaxation function consistent with a dense system of weak moments. In a dense static spin system, the size of the local magnetic field experienced by the muon may depend somewhat on its position in the crystallographic lattice. Although it is well established that the muon binds to an oxygen atom in $\text{YBa}_2\text{Cu}_3\text{O}_{6+x}$ with a muon-oxygen bond length of the order of 1 Å, there is no clear consensus on which of the oxygen sites the muon prefers (26–29).

An important distinction between ZF measurements with $\hat{P}_{\mu}(0) \parallel \hat{c}$ and $\hat{P}_{\mu}(0) \perp \hat{c}$ is that only in the latter configuration is the muon spin polarization relaxed by static internal fields along the \hat{c} -direction of the crystals. Below 45 K, we find that $\lambda_{\perp} > \lambda_{\parallel}$, which implies that the anomalous magnetic field at the muon site is mainly in the \hat{c} -direction, with smaller components in the \hat{a} - \hat{b} plane. From the λ values, we estimate the characteristic field at the muon site to have components of ~ 0.3 G and ~ 0.19 G perpendicular and parallel to the basal plane, respectively. It is important to note that this anisotropy refers to the field at the muon site and does not necessarily imply a similar anisotropy of the spontaneous moments. Thus, one should not necessarily conclude that the field originates from moments preferentially oriented in the \hat{c} -direction.

Figure 3 shows the temperature dependence of the ZF exponential relaxation rate below 200 K in the underdoped $x = 0.67$ sample for the case $\hat{P}_{\mu}(0) \perp \hat{c}$. Over this temperature range, the relaxation rate due to nuclear dipolar broadening is $\Delta_{\perp} = 0.1065 \pm 0.0027 \mu\text{s}^{-1}$. This value is comparable to the value at optimal doping, which suggests that the muon-stopping sites are the same in the underdoped sample. Above 200 K, the line width parameter Δ_{\perp} decreases with increasing temperature, as observed in earlier ZF studies (19). This behavior is attributed to the onset of muon diffusion, resulting in motional averaging of the interaction between the muon and the nuclear dipoles. Below 160 ± 15 K, there is a significant increase in λ_{\perp} . Near this temperature, the Cu spin fluctuation rate is within the neutron time window (10^{10} to 10^{12} s^{-1}) [for example, (7)] and far too fast to be detected with ZF- μSR . Thus, we do not attribute the increased exponential relaxation rate to a growth of the AF Cu spin correlations. At the lowest temperature investigated, the value of λ_{\perp} is substantially smaller than that in the $x = 0.95$ sample, which implies that the spontaneous magnetic fields are weaker. Although this may seem surprising, the trend is consistent with the staggered-flux phase model (15), whereby the magnitude of the orbital currents decreases as the hole concentration decreases. Nevertheless, additional measurements on similar high-quality samples of intermediate oxygen content are certainly need-

ed to clearly establish the dependence of the field strength on the value of x .

We define a temperature T_{ZF}^* at which the onset of spontaneous magnetic fields is observed, and this is plotted versus the oxygen content x along with $T_c(x)$ in Fig. 4. At $x = 0.67$, T_{ZF}^* is between the pseudogap transition $T^* \approx 140$ K determined from the peak in the ^{63}Cu NMR spin-lattice relaxation rate $1/T_1T$ (30) and the departure of the resistivity $\rho(T)$ from linearity (31), and $T^* \approx 200$ K estimated from the downturn in the ^{89}Y NMR Knight shift (32). The hole concentration p can be estimated from the following empirical equation (33)

$$T_c = T_{c,\text{max}}[1 - 82.6(p - 0.16)^2] \quad (2)$$

The inset of Fig. 4 is a plot of T_c and T_{ZF}^* versus the hole concentration p . If one assumes a linear extrapolation through the data points of $T_{ZF}^*(p)$ corresponding to $x = 0.67$ and $x = 0.95$, T_{ZF}^* falls to zero at a critical doped-hole concentration of $p_{\text{cr}} = 0.182 \pm 0.009$.

Our investigation of highly pure and homogeneous crystals of $\text{YBa}_2\text{Cu}_3\text{O}_{6+x}$ reveals the onset of spontaneous static magnetic fields at a temperature dependent on the oxygen content x . In the underdoped sample, the onset is near the pseudogap crossover temperature T^* deduced from other methods, whereas the onset occurs well below T_c at optimal doping. Although the occurrence of magnetic moments below T^* is consistent with some recent theories of the pseudogap phase, the increased ZF relaxation rate is too small to clearly determine whether the static fields arise from a dilute or dense concentration of magnetic moments.

References and Notes

1. R. E. Walstedt, W. W. Warren Jr., *Science* **248**, 1082 (1990).
2. J. M. Tranquada, P. M. Gehring, G. Shirane, S. Shamoto, M. Sato, *Phys. Rev. B* **46**, 5561 (1992).
3. N. Nishida et al., *Jpn. J. Appl. Phys. Pt. 2* **26**, L1856 (1987).
4. N. Nishida et al., *J. Phys. Soc. Jpn.* **57**, 599 (1988).
5. J. H. Brewer et al., *Phys. Rev. Lett.* **60**, 1073 (1988).
6. R. F. Kiefl et al., *Phys. Rev. Lett.* **63**, 2136 (1989).
7. P. Dai et al., *Science* **284**, 1344 (1999).
8. W. W. Warren, *Phys. Rev. Lett.* **62**, 1196 (1989).
9. J. W. Loram, K. A. Mirza, J. R. Cooper, W. Y. Liang, J. M. Wade, *J. Supercond.* **7**, 243 (1994).
10. V. J. Emery, S. A. Kivelson, *Nature* **374**, 434 (1995).
11. J. L. Tallon, J. W. Loram, *Physica C* **349**, 53 (2001).
12. C. Varma, *Phys. Rev. B* **55**, 14554 (1997).
13. ———, *Phys. Rev. Lett.* **83**, 3538 (1999).
14. S. Chakravarty, R. B. Laughlin, D. K. Morr, C. Nayak, *Phys. Rev. B* **64**, 094503 (2001).
15. T. C. Hsu, J. B. Marston, I. Affleck, *Phys. Rev. B* **43**, 2866 (1991).
16. X.-G. Wen, P. A. Lee, *Phys. Rev. Lett.* **76**, 503 (1996).
17. J. B. Marston, A. Sudbø, preprint available at <http://xxx.lanl.gov/abs/cond-mat/0103120>.
18. A. Amato, *Rev. Mod. Phys.* **69**, 1119 (1997).
19. R. F. Kiefl et al., *Phys. Rev. Lett.* **64**, 2082 (1990).
20. Y. Sidis et al., *Phys. Rev. Lett.* **86**, 4100 (2000).
21. H. A. Mook, P. Dai, F. Dogan, preprint available at <http://xxx.lanl.gov/abs/cond-mat/0102047>.
22. The HELIOS spectrometer uses a large superconducting solenoid, so that true ZF measurements could only be obtained at temperatures below T_c where small stray

external fields are excluded from the bulk by the Meissner screening currents flowing around the perimeter of the sample. The LAMPF spectrometer consists of three orthogonal pairs of Helmholtz coils, which allow us to zero the field in the normal state to better than 0.1 G in each of the x , y , and z directions. In the latter setup, a mosaic of single crystals was mounted on a high-purity Ag backing and sandwiched between a thin muon detector and a light guide, all of which was contained within a ^4He gas-flow cryostat. This arrangement ensured that all sources of signal relaxation originated from within the sample.

23. R. Liang et al., *Physica C* **195**, 51 (1992).
24. R. Liang, D. A. Bonn, W. N. Hardy, *Physica C* **336**, 57 (2000).
25. R. Kubo, T. Toyabe, in *Magnetic Resonance and Relaxation*, R. Blic, Ed. (North-Holland, Amsterdam, 1967).
26. J. H. Brewer et al., *Hyperfine Interactions* **63**, 177 (1990).
27. N. Nishida, H. Miyatake, *Hyperfine Interactions* **63**, 183 (1990).

28. N. Weber et al., *Hyperfine Interactions* **63**, 207 (1990).
29. C. Boekema, W. K. Dawson, D. W. Cooke, *Hyperfine Interactions* **86**, 519 (1994).
30. M. Takigawa et al., *Phys. Rev. B* **43**, 247 (1991).
31. B. Wuyts, V. V. Moshchalkov, Y. Bruynseraede, *Phys. Rev. B* **53**, 9418 (1996).
32. H. Alloul, T. Ohno, P. Mendels, *Phys. Rev. Lett.* **63**, 1700 (1989).
33. J. L. Tallon, C. Bernhard, H. Shaked, R. L. Hitterman, J. D. Jorgensen, *Phys. Rev. B* **51**, 12911 (1995).
34. H. Claus, S. Yang, A. P. Paulikas, J. W. Downey, B. W. Veal, *Physica C* **171**, 205 (1990).
35. We gratefully acknowledge S. Chakravarty, J. B. Marston, D. Morr, P. Stamp, I. Affleck, and G. M. Luke for helpful and informative discussions. J.H.B., R.F.K., D.A.B., W.N.H., and R.L. acknowledge support from the Canadian Institute for Advanced Research. C.E.S. acknowledges support from the U.S. Air Force Office of Scientific Research grant F49620-97-1-0297.

19 March 2001; accepted 26 April 2001

Geometric Manipulation of Trapped Ions for Quantum Computation

L.-M. Duan,* J. I. Cirac, P. Zoller

We propose an experimentally feasible scheme to achieve quantum computation based solely on geometric manipulations of a quantum system. The desired geometric operations are obtained by driving the quantum system to undergo appropriate adiabatic cyclic evolutions. Our implementation of the all-geometric quantum computation is based on laser manipulation of a set of trapped ions. An all-geometric approach, apart from its fundamental interest, offers a possible method for robust quantum computation.

The physical implementation of quantum computers requires a series of accurately controllable quantum operations on a set of two-level systems (qubits). These controllable quantum operations can be either of the traditional dynamical origin (1) or of a novel geometric origin (2–7). The all-geometric approach, proposed recently with the name of holonomic quantum computation (4–7), achieves the whole set of universal quantum gates solely based on the Abelian and non-Abelian geometric operations (holonomies), without any contributions from dynamical gates. The holonomies are acquired when a quantum system is driven to undergo some appropriate cyclic evolutions by adiabatically changing the controllable parameters in the governing Hamiltonian (δ –10). The holonomies can be either simple Abelian (commutable) phase factors (Berry phases) or general non-Abelian operations, depending on whether the eigenspace of the governing Hamiltonian is nondegenerate or degenerate. Besides its fundamental interest related

to a general geometric global structure, the holonomic quantum computation scheme has some built-in fault-tolerant features (2, 7), which might offer practical advantages, such as being resilient to certain types of computational errors. Several schemes have been proposed for the geometric realization of the particular conditional phase shift gate with the use of the Abelian Berry phase (2, 3), and one of them has been experimentally demonstrated with the nuclear magnetic resonance technique (2). For a universal quantum computation, one still needs to combine this particular geometric gate with some single-bit dynamical gates (11). We propose an experimentally feasible scheme to achieve the universal quantum computation all by the geometric means. This requires us to realize the non-Abelian holonomies as well as the Abelian ones, because the universal set of quantum gates is necessarily noncommutable. Our scheme, which is based on laser manipulation of a set of trapped ions, fulfills all the requirements for holonomic quantum computation and fits well the status of current technology.

For the holonomic quantum computation proposed recently (4–7), the computational space C is always an eigenspace (highly degenerate) of the governing Hamiltonian, with a

Institute for Theoretical Physics, University of Innsbruck, A-6020 Innsbruck, Austria.

*To whom correspondence should be addressed. E-mail: Luming.Duan@uibk.ac.at